24 [1×12] Wavelength Selective Switches Integrated on a Single 4k LCoS Device

Haining Yang, Peter Wilkinson, Brian Robertson, Sam Giltrap, Oliver Snowdon, Harry Prudden, and Daping Chu

(Top-Scored Paper)

***Abstract*—This article demonstrates the design, assembly, optimisation, and characterisation of 24 [1 × 12] wavelength selective switches (WSSs) based on a single set of optics and a 4k liquid crystal on silicon (LCoS) device. The average insertion loss was measured to be 8.4 dB with an average crosstalk level of 26.9 dB. To our knowledge, this module with 312 fibre ports is the highest-capacity WSS demonstrated so far. The module can be flexibly reconfigured into different switches and port counts for advanced reconfigurable optical add/drop multiplexer (ROADM) applications.**

***Index Terms*—Wavelength selective switch, liquid crystal on silicon.**

I. Introduction

RECONFIGURABLE optical add/drop multiplexers (ROADMs) [1]–[3] have been widely deployed as the core routing technology for modern telecommunication networks [4] and datacentre interconnect (DCI) networks [5]. A typical ROADM system can be divided into the transit part [6] and the add/drop part [7]. The transit part of the ROADM system allows network operators to direct any wavelength-division multiplexed (WDM) signal from any incoming direction to any outgoing direction. The add/drop part enables the wavelength channels to be dropped from the transit part for local processing, or to be added into the network for further transmission. All the routing and add/drop in ROADMs are realised entirely in the optical domain without the need for optical-electrical-optical (OEO) conversion. This makes the modern networks highly energy efficient. State-of-the-art ROADMs are also compatible with the flexible grid standard [8], where wavelength channels are not constrained to the fixed ITU channels slots. This allows the available spectrum in the fibres to be utilised more efficiently and therefore maximises the total capacity of the network. This capability of flexible-grid switching, along with the elimination of OEO conversion, makes ROADM technology future-proof for any signal modulation formats saving subsequent capital expenses (CapEx). Modern ROADMs are therefore expected to be in operation for more than 10 years. The reconfiguration of the ROADM can be done remotely by software, which further reduces the operational expenses (OpEx) for network operators.

Wavelength selective switches (WSSs) [9]–[11] are the key enabling technology for ROADMs. State-of-the-art WSSs use liquid crystal on silicon (LCoS) [12] spatial light modulator (SLM) switching engines in order to support flexible-spectrum switching [13]. As Internet traffic continues to grow exponentially, there is a strong desire to integrate multiple WSSs into a single module, sharing the same optics and LCoS device, for both transit and add/drop part of the ROADM [14]. The transit part of state-of-the-art ROADMs is based on the 'route-and-select' architecture [15], in which multiple WSSs are paired with each other to enable the cross-connecting of WDM channels between different ROADM degrees. For example, 16 WSSs are required in total for the transit part of an eight-degree ROADM. As networks evolve towards increasingly meshed topologies with larger numbers of parallel fibres between the network nodes, the degree count of a ROADM will continue to grow, driving the need for more WSSs. The cost and footprint of the ROADM can be significantly reduced by integrating all or part of those WSSs into a single module. Twin WSS modules [16], [17], which co-package two independent WSSs into a single module, have been commercialised and are widely deployed in the modern ROADMs. Further WSS integration is still desirable, although it may create a single point of failure in a ROADM node. However, the WSSs that are responsible for the parallel fibres from a single direction can be integrated into a single module without causing this issue since the protection scheme is already in place for those fibres [14].

Co-packaged WSS modules are also playing an increasingly important role in the add/drop part of the ROADMs. The add/drop part of the ROADM needs to have colourless, directionless and contentionless (CDC) [18] capabilities in order to realise a fully flexible network operation and therefore maximise the benefit of the ROADM. Conventional CDC add/drop is realised

Manuscript received April 18, 2020; revised June 6, 2020; accepted June 11, 2020. Date of publication June 15, 2020; date of current version February 16, 2021. *(Corresponding author: Daping Chu.)*

Haining Yang is with ROADMap Systems Ltd., St John's Innovation Centre, Cambridge CB4 0WS, U.K., and also with the Display R&D Centre, Southeast University, Nanjing 210000, China (e-mail: haining.yang@roadmapsystems.co.uk).

Peter Wilkinson, Brian Robertson, Sam Giltrap, Oliver Snowdon, and Harry Prudden are with ROADMap Systems Ltd., St John's Innovation Centre, Cambridge CB4 0WS, U.K. (e-mail: peter.wilkinson@roadmapsystems.co.uk; brian.robertson@roadmapsystems.co.uk; sam.giltrap@roadmapsystems.co.uk; oliver.snowdon@roadmapsystems.co.uk; harry.prudden@roadmapsystems.co.uk).

Daping Chu is with ROADMap Systems Ltd., St John's Innovation Centre, Cambridge CB4 0WS, U.K., and also with the Department of Engineering, University of Cambridge, Cambridge CB3 0FA, U.K. (e-mail: dpc31@cam.ac.uk).

Color versions of one or more of the figures in this article are available online at https://ieeexplore.ieee.org.

Digital Object Identifier 10.1109/JLT.2020.3002716

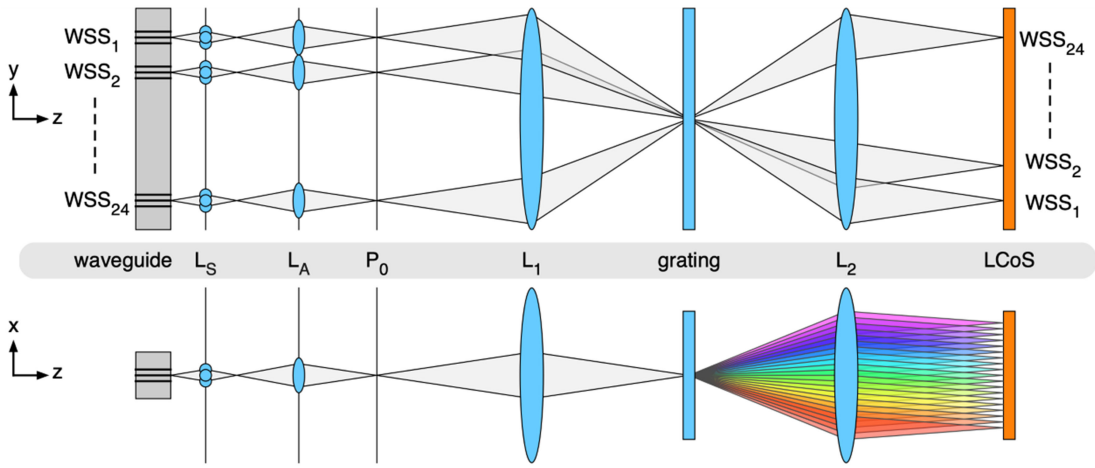

Fig. 1. The optical architecture of stacked WSS module.

by multicasting switches (MCSs) [19], [20], in which an array of passive splitters is paired with an array of space switches. The passive splitters mean that MCSs have poor scalability towards higher port count. MCSs with more than eight drop ports require an additional array of erbium doped fibre amplifiers (EDFAs) to mitigate the excessive insertion loss. This is undesirable from the perspective of the power consumption and the cost. A co-packaged WSS array can replace the splitter array in the MCS and solve the scalability issue, since the insertion loss can be maintained as the port count increases. Pascar et al. [21] first proposed the co-packaged WSS architecture for the CDC add/drop application. Ikuma et al. integrated eight independent 1×24 WSSs and 24 1×8 space switches into a single optical system to realise an 8×24 wavelength crossconnect (WXC) [22], [23] for the same application. The high insertion loss in those demonstrations was significantly reduced by Colbourne et al. [24].

Building on our presentation at OFC 2020 [25], this paper details our technology platform, in which 24 independent 1×12 WSSs are integrated based on a single set of optics and a 4k LCoS device. The 24 WSSs also share the same alignment process, which makes the assembly process highly efficient on a per-WSS basis. The principle of the assembly is similar to that used for a conventional WSS architecture based on 1D beam steering, although the unique 2D beam steering used in this demonstration enables some of the alignment tolerances to be relaxed. The 2D steering also enables the input/output ports to be arranged more densely, reducing the height for the optics for a given port count. The design, assembly, optimisation and characterisation of this WSS system will be detailed in this paper. This architecture can be easily reconfigured for applications in both the transit and add/drop parts of a ROADM.

II. Design of Wavelength Selective Switch

A. LCoS SLM

The system is designed for a 4k phase-only LCoS device that has an active area of 4096×2400 pixels and a pixel pitch of 6.8 μm. The device employs an analogue-voltage driving scheme and is capable of resolving 256 discrete phase levels with a maximum modulation of 2.5π at 1550 nm. Anti-reflection coating and index matching are implemented. To our knowledge, it is the first time that 4k LCoS technology has been successfully demonstrated in a telecommunications application.

B. Optical Design

The optical architecture of the switch module is shown in Fig. 1. It is split into two sections: the input/output optics and the relay system. The input/output optics shown in Fig. 2 contains a linear array of 24 clusters on a 680 μm pitch along the y-axis. Each cluster corresponds to an individual WSS and consists of 13 hexagonally packed ports on an 80 μm pitch, a corresponding collimating lenslet array (L_s), and a Fourier-transform lenslet (L_A). The input WDM channels are launched into each WSS via the central port in the corresponding cluster. This is designed to minimise the required steering angle of the LCoS switching engine. The collimating lenslets, with focal lengths of 0.547 mm, enlarge the effective mode field diameter of the input/output ports. The collimated beam waist is placed at the back focal plane of the lenslet L_A with a focal length of 3.427 mm, which produces a beam waist of 68 μm at its front focal plane (P_o). Compared with a conventional WSS, where the input/output ports are arranged linearly, the 2D arrangement of ports used in this system reduces the overall height of the optics for a given port count by at least 50%, despite it requiring more pixels along the dispersion axis to enable the switching in the second dimension. This is because in a conventional WSS the beam has to be elongated to cover more pixels along the vertical axis for the same port count, assuming the same pitch between ports. This will increase the focal length of the Fourier-transform lens and the height of the optics and holograms.

Plane P_o is also the interface to the relay system. This is a symmetric 4f relay, consisting of two bulk lenses (L_1 and L_2) with focal lengths of 254.5 mm, and a DEMUX diffraction grating (P_g) of 1201 lines/mm placed at the back focal plane of L_1. The relay system images the plane P_o onto the LCoS SLM (P_{SLM}). Since the diffraction grating imparts an angular displacement to each wavelength channel in the x-z plane, the input WDM signals from each WSS will illuminate a spatially distinct row of sub-holograms. The x-axis is hence referred to as the dispersion axis. Sub-hologram rows for adjacent WSSs

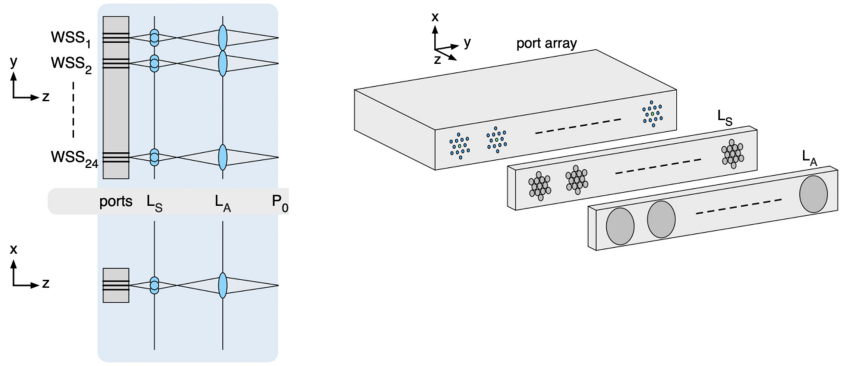

Fig. 2. The detailed design for the input/output optics.

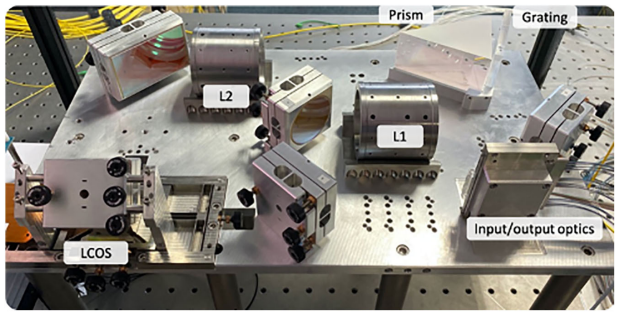

Fig. 3. The experimental setup of the 24 1 × 12 WSS module.

are separated by 100 pixels along the y-axis. The unmodulated input beam covers 30 × 30 pixels on the LCoS device. Adjacent 50 GHz channels are separated by 50 pixels in the x-axis. There are 4096 pixels available along the x-axis of the LCoS device, so the module can cover > 4000 GHz of spectrum. Sub-holograms of 50×50 pixels are displayed on the LCoS device to switch 50 GHz channels. Since each pixel column in the sub-holograms corresponds to 1 GHz, the passband width of this system can be tuned with a resolution of 1 GHz without using the sub-column technique. Each sub-hologram will encode a wavefront pattern to the beam of the corresponding wavelength channel and WSS, which will be subsequently imaged back to plane P_o by the relay optics. Given the telecentric arrangement of the input/output optics, the lenslet L_A associated with each cluster will convert the encoded wavefront tilts to positional offsets with respect to the local input optical axis, whilst L_s ensures the individual wavelength channels are efficiently coupled into the target output fibre ports. The wavefront tilts imparted by the sub-holograms are 2D in nature, corresponding to the hexagonal arrangement of the input/output ports. In addition to increasing the port density, the 2D beam steering used in this system is also capable of compensating for the conical diffraction from the DEMUX grating, and alignment errors. A photograph of this switch is shown in Fig. 3. It can be seen that an additional prism is placed next to the DEMUX grating to linearise the dispersion across the C-band. Five mirrors were also added to shrink the footprint of the system and set the LCoS device flat.

In this specific demonstration module, 24 independent 1 × 12 WSSs are implemented to show the general capability of our technology platform. The switch count and the port count can however be reconfigured for different applications, by changing the design of the input/output optics without any modification to the relay optics. For example, anamorphic optics can be introduced into the input/output assembly to increase the beam size along the y-axis. This would deliver fewer WSSs with higher port count. It should also be noted that polarisation diversity optics are not included in the current module. This functionality could however be easily incorporated by adding a walk-off crystal and a pixelated half-wave plate array at the interface between the input/output optics and the relay system. As the purpose of this work is to demonstrate the feasibility of the technology platform, a transmissive diffraction grating and a relay system based on lenses were used to simplify the alignment procedure. A reflective diffraction grating and curved mirror could be used in this optical architecture to further reduce the footprint of the relay optics.

C. Ultra-High-Density Port Array

The high switching capacity of this demonstration brings the challenge of manufacturing a high-quality 312-port array. In this demonstration, a 3D laser-written waveguide array was used, providing high positional and pointing accuracy. The 312 waveguides were inscribed by a femtosecond laser into a glass substrate [26], [27], inducing a localised change of refractive index inside the glass via a nonlinear absorption process. This ensures an efficient coupling into the single-mode fibres at telecom wavelengths. With the assistance of high-precision multi-axial translation stages, 3D waveguide structures can be formed within the glass. The mode field diameter of these waveguides was designed to be 8.5 μm.

The positions of the 312 waveguides were measured and compared with their targets. The results are shown in Fig. 4(a). The average lateral error in the x-y plane was measured as 0.61 μm. The dashed line in this figure represents the data for a standard 3 × 3 manually aligned fibre array used in our previous demonstration [28]. It can be seen that lateral error is reduced in this waveguide. Figure 4(b) shows the pointing errors of the beams launched from the waveguides into the free space. The black curve and blue curve in this figure were measured before and after the waveguide array was glued to the input/output optics assembly, respectively. Without the input/output optics assembly, the average pointing errors of the waveguide array

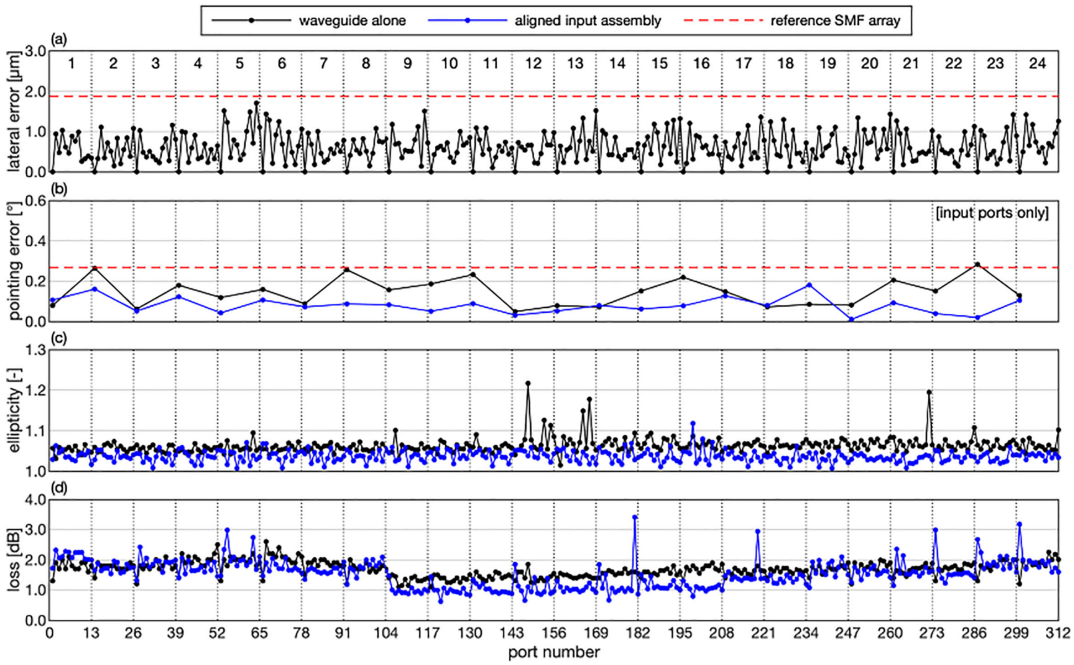

Fig. 4. (a) Lateral positioning errors of the waveguide core positions; (b) pointing errors of the input channel beams to the waveguide facet normal; (c) ellipticity of the free-space beams; (d) insertion losses from the input fibres to the free space beams.

were minimised to 0.15° by carefully polishing the front end of this waveguide array. Compared with the data for the manually aligned fibre array, the pointing error was also reduced in this waveguide array.

To our knowledge, it is also the first time that this type of waveguide is used in free-space optical switching applications. Therefore, the characteristics of beams launched into free space were measured. Figure 4(c) shows that the mean ellipticity was 1.06. There were a small number of waveguides that show relatively large ellipticity. This was due to the surface defects on the waveguide facet. The mean M^2 value for a sample of ports was 1.08, which to within the experimental error is indistinguishable from the 1.10 measured for a single-mode fibre. The insertion loss of each waveguide was also measured, and is shown in Fig. 4(d). The average insertion loss across all channels was 1.69 dB. This is mainly due to the scattering and absorption of the glass substrate, which is around 0.2 dB/cm. In order to minimise the total insertion loss induced by the waveguides, the input waveguides were designed to have shorter path lengths. As a result, the average insertion loss for the connection between input waveguides and output waveguide was calculated to be 3.04 dB. We are also exploring various techniques to further reduce the insertion loss of this input/output port array by using glasses with lower absorption, multi-core fibre [29] array, and high-quality single-mode fibre arrays. The switching technology platform developed in this work is compatible with all these options.

An active alignment procedure was developed to package the waveguide array as a sub-module with the collimating lenslet array and the Fourier-transform lenslet array. Although the port arrangement is 2D in this work, the underlying alignment principle is similar to that for a 1D fibre collimating array. Once the optics corresponding to the top and bottom WSSs are aligned, the remaining 22 WSSs are automatically in the correct position. This makes the alignment process highly efficient on the per-WSS basis. The waveguide array was glued to the collimating lenslet array. The index-matching adhesive between the waveguide and the collimating lenslets reduced the residual surface roughness on the waveguide facet. The beam quality improved as a result, with the average ellipticity dropping to 1.04. Figure 5 shows the packaged input/output optics.

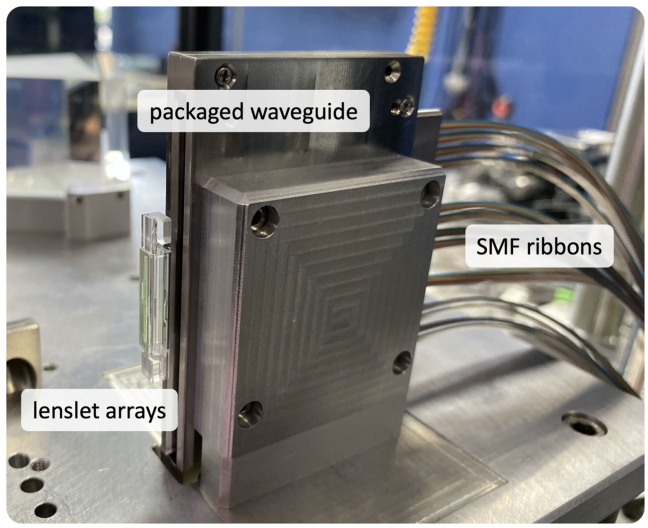

Fig. 5. A detailed view of the input/output optics assembly.

D. 2D Beam Steering

As mentioned in the preceding sections, the use of 2D beam steering in this demonstration increases the achievable port density, allowing more ports to be packed within a given height. In the conventional WSS using 1D beam steering to a linear

array of fibre ports, higher diffraction orders due to defects in the LCoS device overlap with unintended output ports and therefore increase the crosstalk levels. This complicates the hologram optimisation process. In contrast, in this 2D architecture only the -1st diffraction order of the sub-holograms will contribute to the crosstalk, at the port that is symmetrically opposite to the target output port. This significantly simplifies the hologram optimisation and therefore speeds up the process. The 2D beam steering also allows the compensation of certain misalignments and optical defects within the system, including the misalignment between the collimating waveguide ports and the Fourier-transform lenslet array, the distance error between the DEMUX grating and the second relay lens, and the conical diffraction from the DEMUX grating.

In 2D beam steering the phase levels across the sub-hologram dispersion axes are not uniform. This usually introduces significant ripples into the passband, which is unacceptable for ROADM applications. In our previous work [28], [30], this problem was solved by ensuring the periodicity in the sub-holograms along the dispersion axis. In this work, a further a two-stage hologram optimisation procedure was developed to minimise insertion loss and crosstalk across the whole frequency range. Firstly, the period and angle of a standard blazed grating were swept to identify the starting sub-hologram by minimising the insertion loss. Subsequently a high-dimensional optimisation of sub-holograms was performed, using a customised merit function incorporating important parameters such as insertion loss, crosstalk and passband, with appropriate weightings to achieve the best overall performance. This typically achieved an extra crosstalk suppression of 10 dB across the channel bandwidth, at the cost of 0.1 dB of insertion loss. The insertion loss ripple was maintained during this process. A parallel process was developed so that multiple wavelength channels can be optimised at the same time. This significantly increases the speed of our optimisation. We believe that this algorithm is generic and can be applied to different WSS architectures (1D or 2D beam steering). It might however need fine tuning if LCoS devices with significantly different characteristics are used.

III. Experimental Results

The performance of this demonstration was extensively characterised for its insertion loss, crosstalk, and passband, as the key WSS metrics that determine the performance of ROADM networks [31]–[34]. The performance was consistent across all the WSSs integrated in this module. This consistency validates the feasibility of the optical architecture used in this demonstration.

Unfortunately, it was discovered during initial testing that the LCoS device which the switch had been designed for was unable to display the designed holograms properly due to a defect in its backplane circuitry. More specifically, the displayed holograms showed image artefacts, which affected performance, especially the crosstalk levels. As a result, the switch was also tested using a second 4k LCoS device with 4096×2400 pixels and a pixel pitch of 6.4 μm. Due to the 0.4 μm difference in the pixel pitch, the switch count and spectral coverage were slightly reduced. In addition, the reflectivity of the silicon backplane was measured as only ∼64%, which is lower than that obtained previously using 2k panels of the same pixel pitch and fill factor [28]. This will have an impact on the insertion loss values of the switch. In the absence of image artefacts, however, the 6.4 μm 4k panel allowed us to demonstrate our holographic beam steering capability for crosstalk suppression.

TABLE I
Performance of the WSSs

	Device A			Device B		
	Min	Typical	Max	Min	Typical	Max
Insertion loss (dB)	7.2	8.4	10.9	7.7	10.2	15.2
Insertion loss variation across the spectrum (dB)			±0.5			±0.5
Inter-WSS isolation (dB)	45			45		
Intra-WSS isolation (dB)	19.6	26.9	40	20.3	32.3	42
-3 dB passband width for 50 GHz channel (GHz)	42.6	43.4	43.8	41.5	42.8	43.8

TABLE II
The Intrinsic Loss of the WSSs

Component	Transmission	Passes	Loss (dB)
System components (Fresnel losses)	0.92	2	-0.72
Waveguide loss	0.70	2	-3.10
DEMUX grating	0.92	2	-0.72
Intrinsic LCoS reflectivity (A/B)	0.84/0.64	1	-0.72/-1.94
Fibre coupling	0.88	1	-0.56
Total			**-5.82/7.04**

This section will present the detailed switch performance values obtained for both LCoS devices. The original LCoS device will be referred to as Device A while the second device will be referred to as Device B.

A. Insertion Loss

The insertion loss of this demonstration system was measured across the whole supported wavelength range for all the output ports of each stacked WSS. The beam steering sub-hologram for each WSS/port/channel combination was optimised using the algorithm described in the previous section. The experimental results are presented in Table I. A theoretical breakdown of the intrinsic insertion loss of the WSSs is given in Table II. When the diffraction efficiency of the LCoS device is taken into account, the difference between the experimental and theoretical values is small and could be attributed to the misalignment of the system. More importantly, there is no systematic disparity between the WSSs at the centre of the optical axis and those away from it. This shows that the primary aberrations in the relay optics have been successfully minimised. The conical diffraction associated with the DEMUX diffraction grating has also been compensated by the 2D sub-hologram optimisation process. It can also be inferred from Table II that the insertion loss of the system could be significantly reduced if we used an input/output array with lower insertion loss, and a LCoS device with better performance [35]–[37].

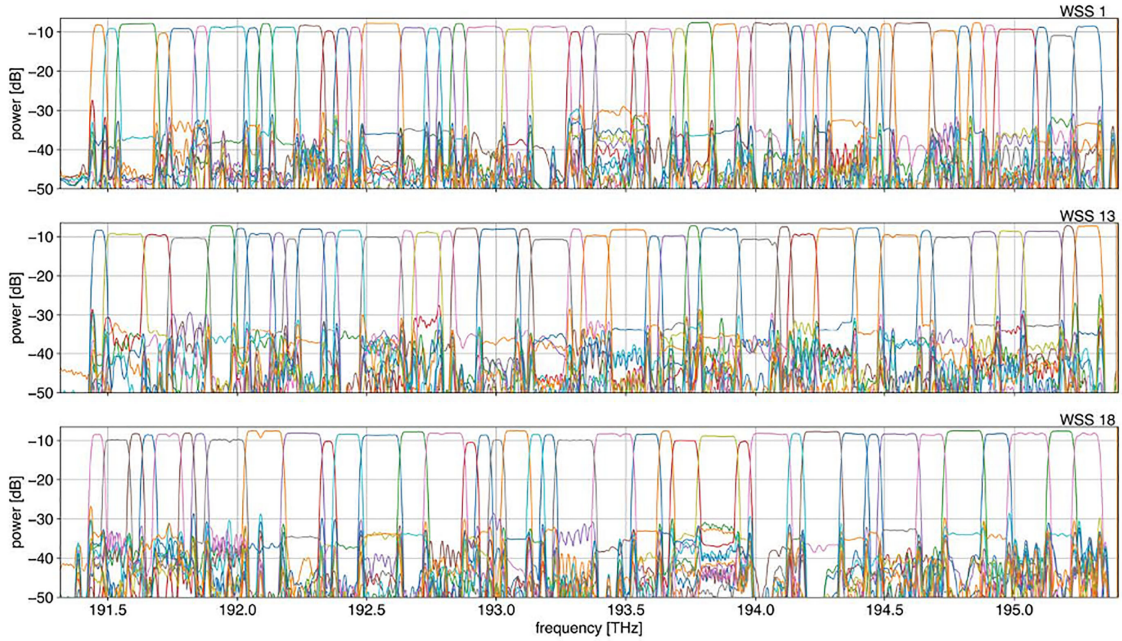

Fig. 6. The representative transmission spectrum at different output ports at different WSS in the system.

B. Crosstalk

The crosstalk within a WSS is defined as the ratio between the power at the target port to the power present at the un-targeted ports. The experimental results are presented in Table I. The crosstalk between WSSs is $<$ -45 dB. This is expected as the only source of such crosstalk in this optical design is scattering, and validates the feasibility of this integrated WSS architecture. As discussed in the previous section, the crosstalk within individual WSSs is primarily due to the -1st diffraction order of the beam-steering hologram at the port that is symmetrically-opposite to the target output port. Crosstalk isolation for this order was up to 40 dB for Device A and 42 dB for device B. This is primarily due to the optical scattering and possibly some misalignment of the system. The experimental results also indicate that the two-stage optimisation algorithm described in the above was effective in suppressing the crosstalk due to the -1st diffraction order. Additional crosstalk suppression could be achieved by further development of the hologram optimisation process, by using the wavefront encoding technique [38], and by improving the performance of the LCoS device.

C. Passband and Flexible-Spectrum Switching

The passband performance was also measured for each WSS. The values of the -3 dB passband width for a 50 GHz channel are given in Table I.

Figure 6 shows the optical power coupled into different output ports for randomly-generated flexible-channel switching patterns based on current standards when the Device B was in use. Each colour corresponds to a different output port within a given WSS. The measured powers are referenced to the input signal. This figure hence also demonstrates the insertion loss and crosstalk for these WSSs, and the consistent performance between WSSs across the integrated module. The insertion loss fluctuations across the spectra are primarily due to the insertion loss variation between output ports. The deep notches in some of the passband curves, and the corresponding peaks in the crosstalk spectra, require further investigation. Possible causes include discontinuities between adjacent sub-holograms with the same target port but different parameters, inclusions in the liquid crystal or scattering off dust.

Figure 6 also demonstrates flexible-spectrum switching. As discussed in the above, each column of pixels is designed to correspond to 1 GHz of spectrum. The passband width can therefore be tuned with GHz granularity by adding or removing pixel columns from the sub-hologram. By utilising the sub-column technique, the resolution could be improved to sub-GHz if needed. This gives our WSSs not only the much-desired full configurability for software-defined networks (SDNs), but also the built-in capability for delivering the granularities of current and future flexible spectrum standards.

V. Conclusion

A highly-integrated WSS technology platform has been demonstrated in the form of a 24 [1 $\times$ 12] WSS module based on a single set of optics and a 4k LCoS device. This demonstration was enabled by our holographic 2D beam-steering capability and a laser-written 3D waveguide array. The holographic 2D beam-steering technique was able to loosen the alignment tolerances and compensate for the conical diffraction effect from the DE-MUX grating. The two-stage holographic optimisation process developed in this work has been shown to provide additional crosstalk suppression while maintaining insertion loss and pass-band performance. The laser-written 3D waveguide provided the 312 port array required for this system. Our characterisation shows that the demonstration has an average insertion loss of -8.4 dB, crosstalk of -26.9 dB and -3 dB passband width of 43.4 GHz. The insertion loss can be further reduced by using port arrays with lower intrinsic loss, while the crosstalk performance

can be improved by further improvements to the hologram optimisation algorithm and implementing the wavefront encoding technique. Both insertion loss and crosstalk can be improved by improving the LCoS performance.

A fundamental advantage of the 2D beam steering architecture is the increase in port density afforded by the 2D port layout. This reduces the volume per port, and hence per WSS. For example, the 2D arrangement of output ports is able to reduce the height of the optics by 50% to 70% for the same port count. Moreover in state-of-the-art standalone or twin WSS modules ∼40% of the module height is used for packaging outside of the optical system. Sharing it among the many WSSs in our stacked architecture could significantly reduce the volume, further increasing the port density on the modular level and hence the switching capacity of a ROADM rack.

The technology platform developed in this work can also be reconfigured into different switch count and port count by only changing the design of input/output optics. This makes this technology platform highly versatile, suitable for applications in both high-degree ROADM transit or scalable CDC add/drop.

REFERENCES

[1] S. Frisken, S. B. Poole, and G. W. Baxter, "Wavelength-selective reconfiguration in transparent agile optical networks," *Proc. IEEE*, vol. 100, no. 5, pp. 1056–1064, May 2012.

[2] P. D. Colbourne and B. Collings, "ROADM switching technologies," in *Proc. Optical Fiber Commun. Conf.*, 2011, Art. no. OTuD1.

[3] S. Gringeri, B. Basch, V. Shukla, R. Egorov, and T. J. Xia, "Flexible architectures for optical transport nodes and networks," *IEEE Commun. Mag.*, vol. 48, no. 7, pp. 40–50, Jul. 2010.

[4] M. D. Feuer, D. C. Kilper, and S. L. Woodward, "ROADMs and their system applications," in *Proc. Opt. Fiber Telecommun. Vol B: Syst. Netw.* (Eds I. P. Kaminow, T. Li, A. E. Willner), Academic Press, San Diego, 2008, Ch. 8, pp. 293–343.

[5] S. J. B. Yoo, Y. Yin, and K. Wen, "Intra and inter datacenter networking: The role of optical packet switching and flexible bandwidth optical networking," in *Proc. 16th Int. Conf. Optical Netw. Design Modelling (ONDM),* 2012, ED-14, pp. 1–6.

[6] M. Filer and S. Tibuleac, "N-degree ROADM architecture comparison: Broadcast-and-select versus route-and-select in 120 Gb/s DP-QPSK transmission systems," in *Proc. Optical Fiber Commun. Conf.*, 2014, Paper Th1I.2.

[7] L. Zong, H. Zhao, Z. Feng, and Y. Yan, "8 x 8 Flexible wavelength cross-connect for CDC ROADM application," *IEEE Photon. Technol. Lett.*, vol. 27, no. 24, pp. 2603–2606, Dec. 2015.

[8] A. Lord, Y. R. Zhou, R. Jensen, A. Morea, and M. Ruiz, *Evolution from wavelength-switched to flex-grid optical networks BT – elastic optical networks: Architectures, technologies and control* V. López and L. Velasco, Eds. Cham: Springer International Publishing, 2016, pp. 7–30.

[9] G. Baxter *et al.*, "Highly programmable wavelength selective switch based on liquid crystal on silicon switching elements," in *Proc. Opt. Fiber Commun. Conf. Expo. Nat. Fiber Opt. Eng. Conf., Tech. Digest (CD)*, 2006, Paper OTuF2.

[10] T. Strasser and J. Wagener, "Wavelength-selective switches for ROADM applications," *IEEE J. Sel. Top. Quantum Electron.*, vol. 16, no. 5, pp. 1150–1157, Sep. 2010.

[11] D. M. Marom *et al.*, "Wavelength-selective 1 x K switches using free-space optics and MEMS micromirrors: Theory, design, and implementation," *J. Lightw. Technol.*, vol. 23, no. 4, pp. 1620–1630, 2005.

[12] Z. Zhang, Z. You, and D. Chu, "Fundamentals of phase-only liquid crystal on silicon (LCOS) devices," *Light Sci. Appl.*, vol. 3, Oct. 2014, Paper e213.

[13] S. Frisken, G. Baxter, D. Abakoumov, H. Zhou, I. Clarke, and S. Poole, "Flexible and grid-less wavelength selective switch using LCOS technology," in *Proc. Opt. Fiber Commun. Conf.*, 2011, Paper OTuM3.

[14] H. Yang, B. Robertson, P. Wilkinson, and D. Chu, "Low-cost CDC ROADM architecture based on stacked wavelength selective switches," *J. Opt. Commun. Netw.*, vol. 9, no. 5, pp. 375–384, 2017.

[15] B. C. Collings, "Advanced ROADM technologies and architectures," in *Proc. Opt. Fiber Commun. Conf. (OFC)*, 2015, Paper Tu3D.3.

[16] 2015. [Online]. Available: https://www.lumentum.com/en/products/trueflex-twin-high-port-count-wavelength-selective-switch-twin-wss

[17] 2017. [Online]. Available: https://www.finisar.com/sites/default/files/downloads/finisar_dual_wss_product_brief_standard_and_low_profile_0917.pdf

[18] Y. Li, L. Gao, G. Shen, and L. Peng, "Impact of ROADM colorless, directionless, and contentionless (CDC) features on optical network performance [invited]," *J. Opt. Commun. Netw.*, vol. 4, no. 11, pp. B58–B67, 2012.

[19] W. I. Way, "Optimum architecture for M×N multicast switch-based colorless, directionless, contentionless, and flexible-grid ROADM," in *Proc. Nat. Fiber Optic Eng. Conf.*, 2012, Paper NW3F.5.

[20] Y. Ma *et al.*, "Novel CDC ROADM architecture utilizing low loss WSS and MCS without necessity of inline amplifier and filter," in *Proc. Opt. Fiber Commun. Conf. (OFC)*, 2019, Paper M1A.3.

[21] L. Pascar, R. Karubi, B. Frenkel, and D. Marom, "Port-reconfigurable, wavelength-selective switch array for colorless/directionless/contentionless optical add/drop multiplexing," in *Proc. Int. Conf. Photon. Switching (PS)*, 2015, pp. 16–18.

[22] Y. Ikuma, K. Suzuki, N. Nemoto, E. Hashimoto, O. Moriwaki, and T. Takahashi, "8 × 24 wavelength selective switch for low-loss transponder aggregator," in *Proc. Opt. Fiber Commun. Conf. Exhib. (OFC)*, 2015, Paper Th5A.4.

[23] K. Suzuki, K. Seno, and Y. Ikuma, "Application of waveguide/free-space optics hybrid to ROADM device," *J. Lightw. Technol.*, vol. 35, no. 4, pp. 596–606, 2017.

[24] P. D. Colbourne, S. McLaughlin, C. Murley, S. Gaudet, and D. Burke, "Contentionless twin 8×24 WSS with low insertion loss," in *Proc. Opt. Fiber Commun. Conf. Expos. (OFC),* 2018, Paper Th4A.1.

[25] P. Wilkinson *et al.*, "24 1×12 wavelength-selective switches using a 312-port 3D waveguide and a single 4k LCoS," in *Proc. Opt. Fiber Commun. Conf. Exhib. (OFC)*, 2020, Paper M3F.2.

[26] N. D. Psaila *et al.*, "Femtosecond laser inscription of optical waveguides in Bismuth ion doped glass," *Opt. Express*, vol. 14, no. 22, pp. 10452–10459, 2006.

[27] D. Choudhury, J. R. Macdonald, and A. K. Kar, "Ultrafast laser inscription: perspectives on future integrated applications," *Laser Photon. Rev.*, vol. 8, no. 6, pp. 827–846, Nov. 2014.

[28] H. Yang, P. Dolan, B. Robertson, P. Wilkinson, and D. Chu, "Crosstalk spectrum optimisation for stacked wavelength selective switches based on 2D beam steering," in *Proc. Opt. Fiber Commun. Conf. (OFC)*, 2018, Paper Th1J.2.

[29] K. Saitoh and S. Matsuo, "Multicore fiber technology," *J. Lightw. Technol.*, vol. 34, no. 1, pp. 55–66, 2016.

[30] H. Yang, B. Robertson, P. Wilkinson, and D. Chu, "Small phase pattern 2D beam steering and a single LCOS design of 40 1x12 stacked wavelength selective switches," *Opt. Express*, vol. 24, no. 11, pp. 12240–12253, 2016.

[31] S. Tibuleac and M. Filer, "Transmission impairments in DWDM networks with reconfigurable optical add-drop multiplexers," *J. Lightw. Technol.*, vol. 28, no. 4, pp. 557–568, 2010.

[32] T. Zami, B. Lavigne, and E. Balmefrezol, "Crosstalk analysis applied to Wavelength Selective Switches," in *Proc. Opt. Fiber Commun. Conf. (OFC)*, 2006, Paper OFP4.

[33] C. Pulikkaseril, L. A Stewart, M. A F. Roelens, G. W. Baxter, S. Poole, and S. Frisken, "Spectral modeling of channel band shapes in wavelength selective switches," *Opt. Express*, vol. 19, no. 9, pp. 8458–8470, Apr. 2011.

[34] H. Yang *et al.*, "Impact of WSS passband narrowing effect on the capacity of the flexible-spectrum networks," in *Proc. Opt. Fiber Commun. Conf. (OFC)*, 2017, Paper W1I.5.

[35] Z. Zhang *et al.*, "High quality assembly of phase-only liquid crystal on silicon (LCOS) devices," *J. Disp. Technol.*, vol. 7, no. 3, pp. 120–126, 2011.

[36] H. Yang and D. P. Chu, "Phase flicker optimisation in digital liquid crystal on silicon devices," *Opt. Express*, vol. 27, no. 17, pp. 24556–24567, 2019.

[37] H. Yang and D. P. Chu, "Digital phase-only liquid crystal on silicon device with enhanced optical efficiency," *OSA Contin.*, vol. 2, no. 8, pp. 2445–2459, 2019.

[38] B. Robertson *et al.*, "The use of wavefront encoding to reduce crosstalk in a multicasting fiber telecom switch," in *Proc. Opt. Fiber Commun. Conf. (OFC)*, 2012, Paper OM2J.6.